# Proceedings of The Sixth International ZEOLITE Conference

CONTENTS

## DON BRECK MEMORIAL SYMPOSIUM


| | | |
|---|---|---|
| 1. | The Word and Work of Don Breck.<br>E. M. Flanigen | 3 |
| 2. | Zeolite Synthesis: Some Chemical Aspects.<br>R. M. Barrer. | 17 |
| 3. | Adsorption in A, X and Y Zeolites: Thirty Years of Science and Technology.<br>D. M. Ruthven. | 31 |
| 4. | Speculations on Molecular Sieve and Ionization Effects in Y Zeolite.<br>J. A. Rabo. | 41 |
| 5. | Considerations on Some Effects of Cation Location in the Faujasite-Type Zeolites.<br>J. B. Uytterhoeven. | 49 |
| 6. | New Vistas in Crystal Structures of Molecular Sieves and Some Personal Reminiscences of Donald W. Breck.<br>J. V. Smith. | 56 |
| 7. | Zeolite Exploration: The Early Days.<br>F. A. Mumpton. | 68 |
| 8. | Zeolite Chemistry V - Substitution for Aluminum in Zeolites via Reaction with Aqueous Ammonium Fluorosilicate.<br>G. W. Skeels and D. W. Breck. | 87 |
| 9. | Synthesis of $AlPO_4$ Molecular Sieves.<br>S. T. Wilson, B. M. Lok, C. A. Messina and E. M. Flanigen. | 97 |
| 10. | Studies on the Prediction of Multicomponent Ion-Exchange Equilibria Involving Natural and Synthetic Zeolites.<br>R. P. Townsend, P. Fletcher and M. Loizidou. | 110 |
| 11. | Diffusional Transition in Zeolite NaX:<br>1. Single Crystal Gas Permeation Studies.<br>D. L. Wernick and E. J. Osterhuber. | 122 |
| 12. | The Cation Distribution in Faujasites.<br>M. J. Sanders and C. R. A. Catlow. | 131 |
| 13. | Statistical and Topological Approaches to Modelling Zeolite Acidity, Activity and Stability.<br>W. A. Wachter. | 141 |
| 14. | Agglomeration Mechanism During the Preparation of Ni(0) and Fe(0) Zeolites.<br>F. Schmidt, Th. Bein, U. Ohlerich and P. A. Jacobs. | 151 |
| | Discussion | 161 |

## ADSORPTION - DIFFUSION


1. Experimental and Theoretical Analysis of the Adsorption of Methane in A Zeolites: Infrared and Neutron Spectroscopy Studies. 172
E. Cohen De Lara and R. Kahn.

2. NMR Diffusion Studies in Zeolites. 184
J. Karger, H. Pfeifer and W. Heink.

3. Investigations of Motion, Interaction and Oxidation of Carbon Monoxide in Alkali and Alkaline Earth Ion-Exchanged Zeolite A. 201
H. Bose, H. Forster, W. Frede and M. Schumann.

4. Gas Chromatographic Sorption Studies of Hydrocarbons in Pentasils with Different Si/Al Ratios. 210
H. Lechert and W. Schweitzer.

5. Direct Measurement of Diffusivity for Butane Across a Single Large Silicalite Crystal. 217
A. Paravar and D. T. Hayhurst.

6. Experimental and Theoretical Investigations of the Adsorption of n-Paraffins, n-Olefins and Aromatics on Silicalite. 225
H. Stach, H. Thamm, J. Janchem, K. Fiedler and W. Schirmer.

7. Diffusional Transition in Zeolite NaX: 2. Polycrystalline Gravimetric Sorption Studies. 232
O. H. Tezel, D. M. Ruthven and D. L. Wernick.

8. Diffusion of Benzene in NaX Zeolite. 242
M. Bulow, W. Mietk, P. Struve, W. Schirmer and M. Kocirik and J. Karger

9 The Effect of Cation on Adsorption and Diffusion in ZSM-5. 251
P. Wu and Y. H. Ma.

10. Temperature Programmed Water Desorption of Zeolites. 2. Alkali Metal and Alkaline Earth Cationic Forms of Zeolite X. 261
W. A. McCann and L. V. C. Rees.

11. Adsorption of $C_8$ Aromatics on NaY Zeolite. 268
M. Goddard and D. M. Ruthven.

12. Zeolite RHO. Part III. Sorption of Inorganic Gases and Hydrocarbons. 276
R. M. Barrer and M. A. Rosemblat.

13. The Use of Isopiestic Vapour Pressure Measurements to Study Salt Imbibition by Zeolites. 288
S. G. Fegan and B. M. Lowe.

Discussion 298

## GENERAL ACID CATALYSIS


1. Dehydration of Cyclohexanol as a Test Reaction for Zeolite Acidity. .. 308
H. G. Karge, H. Kosters, and Y. Wada.

2. Relation Between Acidic Properties and Catalytic Performance For Gasoline Synthesis from Methanol Over ZSM-5 Class Zeolites. 316
T. Inui, H. Matsuda, and Y. Takegami.

3. Factors Influencing the Selectivity in the Ethylation of Toluene Over ZSM-5 Zeolites. 325
K. H. Chandavar, S. G. Hegde S. B. Kulkarni, P. Ratnassamy, G. Chitlangia, A. Singh and A. V. Deo.

4. Isomerization-Disproportionation of M-Xylene Over Dealuminated Mordenites. 331
N. Giordano, P. Vitarelli, S. Cavallaro, R. Ottana and R. Lembo.

5. Modified Mordenites for Catalytic Conversion of Methanol. 337
J. Bandiera, C. Hamon, and C. Naccache.

Discussion 345


## METAL CATALYSIS


1. Physical and Catalytic Properties of Noble Metals in Zeolites. 352
P. Gallezot.

2. Structural and Catalytic Properties of Zeolite-Supported Cu-Pt, Cu-Ir, Cu-Rh, and Cu-Ru Bimetallic Clusters. 368
I. Tebassi, A. M. Satarum, A. Ghorbel, M. Dufaux, Y. Ben Taarit.

3. Nickel Sulfides in X-Type Zeolite. 377
D. Cornet, A. Ezzamarty, and J. F. Hemidy.

4. Mechanisms of Reduction and Metal Particle Growth in $Ni^{2+}$, $Pd^{2+}$, and $Pt^{2+}$ Exchanged Faujasites. 387
D. Exner, N. I. Jaeger, R. Nowak, G. Schulz-Ekloff and P. Ryder.

5. Characterization and Reactivity of Nickel Loaded Mordenite Towards the CO+NO Reaction. 396
E. Garbowski, M. Primet and M. V. Mathieu.

6. Preparation and Characterization of Molybdenum Zeolites. 405
Mark B. Ward and J. H. Lunsford.

7. Intrinsically Corrected XP Spectra of Zeolites at Elevated Temperatures: XPS Study of Ni Containing A, X, Y, and ZSM-5 Zeolites. 417
F. Steinbach, J. Schutte, R. Krall, Chr. Minchev, V. Kanazirev, and V. Penchev

8. n-Alkane Transformation, Activity and Stability of Platinum-Zeolites. 427
G. Perot, P. Hilaireau and M. Guisnet.

9. Synthesis, Characterization and Catalytic Properties of Rhodium Carbonyl Cluster Compounds Within Y Zeolite Cages. F. Lefebvre, P. Gelin, C. Naccache and Y. Ben Taarit. 435

10. Hydrosulfurization of the C=C Bond on $Me^{2+}$ -Zeolites. D. Kallo, G. Onyestyak and J. Papp, Jr. 444

Discussion 454

## PENTASIL CATALYSIS

1. Acid Catalysis With Medium Pore Zeolites. W. O. Haag. 466

2. Correlation Between the Sorptive and Catalytic Properties of a Series of Pentasil Zeolites. I. D. Harrison, H. F. Leach and D. A. Whan. 479

3. The Reaction Mechanism of the First C-C Bond Formation in the Methanol to Gasoline Process. J. H. C. van Hooff, J. P. van den Berg, J. P. Wolthuizen and A. Volmer. 489

4. Shape Selectivity and Acidity of ZSM-5 and ZSM-11 Type Zeolites. J. C. Vedrine, A. Auroux, G. Coudurier, P. Engelhard, J. P. Gallez and G. Szabo. 497

5. Shape Selectivity of Pentasil-Type Zeolites in the Bifunctional Conversion of Ethylbenzene and Propylbenzene. R. C. Sosa, M. Nitta, H. K. Beyer and P. A. Jacobs. 508

6. Diffusion and Catalytic Reaction of 2, 2-Dimethylbutane in ZSM-5 Zeolite. M.F.M. Post, J. Van Amstel and H.W. Kouwenhoven 517

7. Sorption and Catalytic Reaction in Different Preparations of Zeolite HZSM-5. J. Herring and L. Riekert and L. Marosi 528

8. Ammoxidation of Toluene and Related Aromatics over Zeolite ZSM-5. A New Application of Zeolite ZSM-5. J. C. Oudejans, F. J. van der Gaag and H. van Bekkum 536

9. Aluminosilicate and Borosilicate Zeolites and Their Use in the Conversion of Methanol to Olefins. W. Holderich, H. Eichorn R. Lehnert L. Marosi, W. Mross, R. Reinke, W. Ruppel and H. Schlimper 545

Discussion 556

## GEOLOGY AND MINERALOGY


1.. Mineralogy of Natural Zeolites: Present Status. 570
R. Rinaldi.

2.. Zeolite Occurrences in Triassic-Jurassic Sedimentary Rocks, Baja California Sur, Mexico. 584
D. A. Barnes, J. R. Boles and J. Hickey.

3.. Diagenetic Zeolite Zone Modified by Recent High Heat Flow in Miti-Kuromatsunai Hole, Southwest Hokkaido, Japan. 595
A. Iijima, K. Aoyagi and T. Kazama.

4.. Zonal Distribution of Zeolites and Authigenic Plagioclase. 604
M. Utada and J. D. Vine.

5.. Thermodynamic Studies of Zeolites. Analcime Solid Solutions. 616
W. S. Wise.

Discussion 623


## ION EXCHANGE


11. Binary and Ternary Cation Exchange in Zeolite A. 626
L. V. C. Rees.

22. Thermodynamic Stability of the Silver-Pyridine Complex in Zeolite Y. 641
E. Rasquin, A. Maes and A. Cremers.

33. Pore Size Engineering by Modifying the Zeolitic Pore system of Mordenite. 651
G. Peeters, A. Thys, E. F. Vansant and P. DeBievre.

44. Evaluation of Zeolite Mixtures for Decontamination of High-Activity-Level Water in the Submerged Demineralizer System (SDS) Flowsheet at the Three Mile Island Nuclear Power Station, Unit 2. 660
L. J. King, D. O. Campbell, E. D. Collins, J. B. Knauer and R. M. Wallace.

Discussion 669


## NEW TECHNIQUES


11. Surface Properties of Offretite and ZSM-34 Zeolites. 674
M. L. Occelli, R. A. Innes, T. M. Apple and B. C. Gerstein.

22. Study of Cation Effects in LiNaA Zeolites by Silicon-29 and Lithium-7 NMR. 684
M. T. Melchior, D. E. W. Vaughan, A. J. Jacobson and C. F. Pictroski.

3. A High Resolution Solid State $^{13}C$ NMR Investigation of Occluded Templates in Pentasil-Type Zeolites; Some $^{29}Si$ Solid State NMR Characteristics of ZSM-5
G. Boxhoron, R. A. van Santen, W. A. van Erp, G. R. Hays, N. C. M. Alma, R. Huis and A. D. H. Clague. 694

4. The Application of Fast Atom Bombardment Mass Spectrometry (FABMS) to the Study of Zeolites.
A. G. Ashton, J. Dwyer, I. S. Elliott, F. R. Fitch, G. Qin, M. Greenwood and J. Speakman. 704

5. A Non-Empirical Molecular Orbital Study of the Siting and Pairing of Aluminum in Mordenite.
E. G. Derouane and J. G. Fripiat. 717

Discussion 727

**STRUCTURE**

1. Structural Chemistry of Zeolites: the Interface Between Structure and Activity.
W. J. Mortier. 734

2. Recent Results in Structural Studies of Zeolites and Zeolite-Like Materials.
S. Merlino. 747

3. Zeolites: The Future.
G. T. Kokotailo. 760

4. Influence of Thallium Ion on Cupric Ion Locations in Cu-TlX Zeolite Studied by Electron Spin Resonance and Electron Spin Echo Modulation Spectrometry.
M. Narayana and L. Kevan. 774

5. Study of the Dealumination and Realumination of ZSM-5 Type Zeolites by $^{29}Si$ and $^{27}Al$ High Resolution Magic Angle Spinning NMR Spectroscopy.
P. A. Jacobs, M. Tielen, J. B. Nagy, G. Debras, E. G. Derouane, and Z. Gabelica. 783

6. High Resolution Electron Microscopic and Optical Diffractometric Studies of Zeolites.
G. R. Millward, J. M. Thomas, S. Ramdas and M. T. Barlow. 793

7. Three Dimensional Mapping of the Zoned Aluminum Distribution in ZSM-5.
R. von Ballmoos, R. Gubser and W. M. Meier. 803

8. The Effect of Dehydration upon the Crystal Structure of Zeolite RHO.
L. B. McCusker and C. Baerlocher. 812

9. The Possibilities and Limitations of the Powder Method in Zeolite Structure Analysis. The Refinement of ZSM-5.
C. Baerlocher. 823

10. Topological Changes in Dehydrated Zeolites: Breaking of T-O-T Bridges. 834
A. Alberti and G. Vezzalini.

11. Neutron and X-ray Refinements of Scolecite. 842
J. V. Smith, J. J. Pluth, G. Artioli and F. K. Ross.

12. Framework Topology and Systematic Derivation of Zeolite Structures. 851
M. Sato.

Discussion 858

## SYNTHESIS

1. Isomorphous Replacements in Zeolites and Other Tectosilicates. 870
R. M. Barrer.

2. Determination of Boundary Conditions of Crystallization of ZSM-5 - ZSM-11 in One "Al-Free" System. 887
L. Y. Hou and L. B. Sand.

3. The Synthesis and Characterization of Zeolite EU-1. 894
J. L. Casciand, T. V. Whittam and B. M. Lowe.

4. Crystallization of Zeolite Y from Solution Phase. 905
S. Ueda, N. Kageyama and M. Koizumi.

5. On the Use of Multinuclear High Resolution Solid State NMR Spectroscopy to Characterize Intermediate Phases Formed During ZSM-5 Zeolite Synthesis. 914
Z. Gabelica, J. B. Nagy, G. Debras and E. G. Derouane.

6. $^{27}Al$ and $^{29}Si$ NMR Studies of Aluminosilicate Species in Solution. 925
L. S. Dent Glasser and G. Harvey.

Discussion 934

## ZEOLITE TECHNOLOGY

1. The Use of Sodium Type A Zeolite in Laundry Detergents. 940
R. A. Llenado.

2. Self-Bonded Phillipsite Pellets From Trachytic Products. 957
R. Aiello, C. Colella, A. Nastro, and R. Sersale.

3. Effects of Surfactant Structure on Detergency Performance of Laundry Powders Formulated with Zeolite 4A as Builder. 966
L. Kravetz.

4. Use of Zeolite NaA for Removal of Trace Heavy Metals from Metal Plating Wastewater. 975
E. P. Hertzenberg.

Discussion 984

GEOLOGY AND MINERALOGY AD HOC MEETING 985

POSTER PAPERS 986

DEPOSITORY OF SUPPLEMENTARY MATERIAL 990

AUTHOR INDEX 991

SUBJECT INDEX 995

# AGGLOMERATION MECHANISM DURING THE PREPARATION OF Ni(0) AND Fe(0) ZEOLITES

F. Schmidt, Th. Bein, U. Ohlerich and P. A. Jacobs*

Institut für Physikalische Chemie der Universität Hamburg, Laufgraben 24, D-2000 Hamburg 13 (F.R.G.)

* Centrum voor Oppervlaktescheikunde en Colloidale Scheikunde, Katholieke Universiteit Leuven, De Croylaan 42, B-3030 Heverlee (Belgium)

Magnetization measurements have been used to study the reduction process of Ni-zeolites and the thermal decomposition of iron pentacarbonyl adsorbed on NaY zeolites. The Ni(0) particle size distribution in $H_2$-reduced NiNaA, NiNaX, NiNaY and NiNaM is bidisperse. The amount and the volume of particles exceeding the cage dimensions increases in the sequence M,Y,X,A zeolites. Particle fusion is found to be the rate determining step. With decomposition of $Fe(CO)_5$/NaY adducts, up to 97 wt.% of the iron particles produced are smaller than 1.3 nm. Fluidized sample bed, inert gas atmosphere and fast heating up to 440 K are essential to reach mononodal dispersion.

## INTRODUCTION

Transition metal containing zeolites are very promising catalysts for petrochemical reactions (1). The metal phase introduced into the zeolite pore system (2) is subject to particle growth or 'sintering'. Since total active metal surface area is influenced considerably by this effect, knowledge is desirable about agglomeration mechanisms of metal species supported on zeolites.

In general, the formation of an initial metal dispersion during preparation must be distinguished from the particle growth under catalytic conditions. Because of the complexity of the latter process, the present study is concerned with thermally activated agglomeration phenomena in the absence of reactants.

The influence of the preparation method will be treated by means of two completely different ways of introducing the metal:

- nickel(0) zeolite is prepared by ion exchange, dehydration and subsequent reduction by molecular hydrogen,
- iron(0) zeolite is obtained by absorption and thermal decomposition of iron pentacarbonyl.

The latter preparation method has been chosen in order to avoid possible contamination with the strong reducing agents required to reduce iron(II) zeolites, e.g. alkali metal vapour (3) or atomic hydrogen.

## EXPERIMENTAL

### 1. Materials

The starting materials for the Ni samples were: Linde A zeolite (Si/Al = 1) and NaY (Si/Al=2.46), NaX (Si/Al=1.18) and Na-mordenite (Si/Al=5.41) from Norton, which is referred to as NaM. The stoichiometrically Ni(II) exchanged samples were dehydrated in a stream of argon (9.5 $cm^3$ $min^{-1}$) by heating up to 823 K (heating

Table I

Decomposition conditions for the iron zeolites

| Sample[a] | Pressure/ mbar | Heating rate/ $K \cdot min^{-1}$ | max. temp./ K | Outgassing/[b] hours |
|---|---|---|---|---|
| FeY0SB | $10^{-4}$ | 0.2 | 373 | 14 |
| FeY480FB | He, 480 | 15 | 445 | 5 |
| FeY17FB | He, 17 | 15 | 420 | 5 |
| FeY0FB | $10^{-2}$ | 15 | 410 | 5 |

a: SB: fixed shallow bed; FB: fluidized bed conditions

b: performed at a temperature of 373 K and a pressure of $10^{-4}$ mbar

Table II Approximate PSD of Ni(O) in various zeolites as a function of the temperature of reduction ($T_R$)

| | | wt % of particles in different size fractions ($V^{1/3}$/nm ): | | | |
|---|---|---|---|---|---|
| | | <0.5 | 0.5 | 1.0 | 2.0 - 8.0 |
| Sample | $T_R$ | 1 | 2 | 3 | 4 |
| NiNaM | 573 | 72.6 | 5.8 | 0 | 21.6 |
| | 723 | 71.7 | 5.5 | 1.0 | 21.8 |
| | 773 | 74.9 | 1.8 | 1.4 | 21.9 |
| | 823 | 71.7 | 3.7 | 2.9 | 21.7 |
| NiNaY | 623 | 35.1 | 17.0 | 22.5 | 25.4 |
| | 673 | 37.3 | 13.7 | 23.7 | 25.3 |
| | 723 | 37.0 | 14.0 | 18.0 | 31.0 |
| | 773 | 39.8 | 14.3 | 16.7 | 29.2 |
| NiNaX | 623 | 57.6 | 0 | 32.2 | 10.2 |
| | 673 | 34.7 | 0 | 28.7 | 36.6 |
| | 723 | 36.8 | 0 | 22.0 | 41.2 |
| | 773 | 21.9 | 4.5 | 25.9 | 47.7 |
| NiNaA | 823 | 3.2 | 26.4 | 0.3 | 70.1 |

rate: 11 K/min), maintaining the samples at that temperature for 4 hours and then cooling down to room temperature during 90 minutes. All samples were reduced in flowing hydrogen (10 $cm^3$ $min^{-1}$) for two hours at elevated temperatures between 573 and 823 K. The final Ni weight content was: NiNaA = 7.8 wt % Ni; NiNaX = 7.3 wt % Ni; NiNaY = 5.5 wt % Ni and NiNaM = 5.9 wt % Ni.

For the preparation of iron zeolites, synthetic NaY from Strem Chemicals (Si/Al=2.46) was used. All treatments were performed in a greaseless reaction system with a heatable quartz bulb of 5mm diameter, connected to a buffer volume of 1 $dm^3$, a $Fe(CO)_5$ reservoir and a high vacuum line. The samples completely dehydrated were loaded at 293 K with predistilled dry $Fe(CO)_5$ (Ventron) at a partial pressure of 8 mbar for 5 hours in the dark. Decomposition of the sorbed carbonyl was performed after evacuation for 2 hours at $10^{-4}$ mbar in static shallow bed (SB) or in fluidized bed conditions (FB). The fluidized bed was generated by horizontal vibration at 50 Hz with an amplitude of 2 mm. Conditions of decomposition are listed in Table I.

## 2. Methods

A Faraday balance was used in the temperature range from 6 - 300 K and fields up to 1 T. Some samples have been measured using a Foner magnetometer in the temperature range from 2.2 K to 200 K and fields up to 8 T. After preparation, all sample bulbs were sealed off under high vacuum. These bulbs were directly used for measurements of the magnetization. Electron microscopy was performed with an analytical TEM-SCAN 100S from Jeol. The Ni-samples were embedded in Spurr® (air free) and cut with an ultramicrotome. Deep frozen Fe-samples were carefully contacted with air, suspended in EtOH, placed on a grid and dried.

# RESULTS AND DISCUSSION

## 1. Evaluation of the Magnetic Measurements

The metallic particle size distribution, PSD, was determined by analyzing the magnetization isotherms. In metal zeolite systems, the measured magnetization can be approximated by

$$\frac{\sigma}{\sigma_\infty} = q_1 L\left(\frac{M_s v_1 B}{kT}\right) + q_2 L\left(\frac{M_s v_2 B}{kT}\right) \ldots + q_i L\left(\frac{M_s v_i B}{kT}\right)$$

with $L(x) = \coth(x - 1/x)$ and $x = M_s v_i B/(kT)$. $\sigma$ is the specific magnetization at the field B and the temperature T, $\sigma_\infty$ is the specific saturation magnetization at the temperature T, $v_i$ is the volume of the particle i, $M_s(T)$ is the spontaneous magnetization at the temperature T.

In cases of a bidisperse or multidisperse PSD, the superposition of the single Langevin isotherms cannot be obtained. This is the normal situation in metal zeolite systems. Here, the analysis of the low temperature/high field isotherm is more sensitive to the smallest particles and the high temperature/low field isotherm is sensitive to the larger particles (4). Usually, the low field volume $v_{LF}$ and the high field volume $v_{HF}$ are taken from the magnetization isotherm at one temperature (5). The exact expression will be low argument volume $v_{LA}$ and high argument volume $v_{HA}$ depending on whether $x = (m_s vB)/kT$ is much smaller than unity or much larger than 4 (magnetic saturation). If all particle fractions - even the smallest ones - are magnetically saturated ($x_i > 4$), the calculated mean particle volume $v_{HA}$ is independent of the form of the actual PSD - function. Depending on the PSD present, suitable temperatures must be choosen for the

analysis of the magnetization isotherms in order to include all particles. In summary, the analysis of the magnetization isotherm at low temperatures gives the PSD and hence $v_{HA}$ and at high temperatures the PSD and $v_{LA}$.

At temperatures as low as 6 K and fields smaller than 1 T the magnetization isotherm $\sigma(B)$ is linear for ions, charged clusters, and particles smaller than about 0.5 nm as well. As a consequence, these three species cannot be distinguished. This is important for incompletely reduced samples or for electron deficient clusters. Therefore in such samples these three fractions are regarded as one single fraction, referred to as PS (paramagnetic species).

## 2. Formation of Ni Particles During Reduction with $H_2$

The PSD of Ni(0) in A, X, Y, and M zeolites obtained upon reduction at various temperatures are given in Table II. For all samples a large amount of paramagnetic species is found (column 1), increasing from A zeolite to mordenite.

The fraction of Ni particles smaller than the dimensions of the zeolite cages ranges from 60% to 90% with the exception of NiNaA. The amount of the larger particles at high temperatures of reduction increases in the sequence M < Y < X < A (see column 4).

Metal particle growth can occur during thermal treatment by two distinct mechanisms. The model developed by Pulvermacher and Ruckenstein (5,6) describes the sintering process by the migration of metal crystallites over the support surface followed by coalescence with other metal crystallites upon collosion (crystallite migration - CM model).

Mass transfer is proposed to proceed by two different mechanisms: Large particles migrate by a momentary accumulation of metal atoms on one side resulting in a movement in the corresponding direction (7). In contrast, very small clusters can migrate as an unperturbed unit.

According to the atomic migration model (AM model) proposed by Flynn and Wanke (8), single metal atoms are transferred individually from one particle and are deposited on the growing particle. In this case gas phase diffusion and surface diffusion can be regarded as well.

Since the bonding energies of Fe or Ni metal atoms to the metal crystallites are much larger than the bonding energies of the metal atoms to the zeolite support, the AM model is unlikely except for very high temperatures and/or charged clusters (see below).

All samples exhibit a bidisperse PSD. Since there may be different mechanisms of sintering, depending on the size of the particles, the nodes will be discussed separately with respect to the sintering models mentioned above.

The fraction of paramagnetic species (PS) can be formed as follows:

a. Incomplete reduction of Ni(II) ions which remain then in hidden sites or in sites, where they can merge with reduced Ni(0) atoms, in this way forming charged clusters. The latter are expected to show strong particle support interaction due to the electrostatic forces.

b. Reaction of Ni(0) with hydroxyl groups of the zeolite (9), or with the acid centers formed during $H_2$ reduction. At higher temperatures these centers also can be dehydroxylated. The water thus formed can oxidize the metal. The metal surface finally can be passivated by a surface layer of oxide/hydroxide.

The second way of sintering should lead to an increase of the PS at the expense of the metallic particles. On the other hand, further reduction can increase the PS too. Hence, evidence for this mechanism can only be obtained if the amount of large particles decreases upon sintering. This is not found in NiNaM and in NiNaX. Only in NiNaY this may be a possible mechanism. The high number of PS and the small changes in their amount in NiNaM and NiNaY indicate a resistance towards sintering due to a strong interaction of the zeolite with the charged clusters (way 1). In this case, sintering can only proceed according to the AM model. The fraction of particles with $v^{1/3}$ greater than 0.5 nm can migrate according to the AM model or CM model as well. None of these models, however, can explain the enormous increase of the number of large particles in NiNaX as compared to NiNaY.

## 3. A Model for Particle Growth in Matrix Dislocations

Electron micrographs of a large number of reduced nickel zeolites always show local distortions of the matrix, though the samples seem to be completely "crystalline" as evidenced by x-ray diffraction. Fig. 1 gives an example of NiNaY zeolite, reduced at 673 K. Along the one-dimensional defect, the particles can migrate easily. Assuming that the formation of defects in the matrix is the main influence on the rate of sintering, one would expect that particle growth should increase in the sequence M<Y<X<A zeolite, as a result of the decreased thermal stability of the protonic forms of these zeolites which are generated upon reduction. The results given in Table II confirm this assumption. The AM model cannot explain the differences in PSD between A-, X-, Y- and M-zeolites and can be rejected for the diffusion through channels (see above) or along a defect path. The sintering can occur by crystal migration along the defect path in case of large particles and through the channels in case of small particles.

It remains to be answered whether the particle growth will be sintering controlled (fusion controlled) or diffusion controlled. For high temperatures diffusion will be rapid and the aggregation is expected to be the rate determining step. This is a reasonable assumption if the matrix has to be destroyed by the growing particle. According to Ruckenstein and Pulvermacher (6), magnetic measurements can be used to decide between sintering control and diffusion control. High values of the ratio $v_{HA}/v_{LA}$ indicate sintering control. Excluding the paramagnetic species the mean particle size defined as

$$v_{HA} = \sum_i \frac{q_i v_i}{\sum_i q_i}$$

was found to be 3.2 nm in NiNaY, reduced at 723 K and measured at 6 K. The corresponding low argument mean particle volume

$$v_{LA} = \sum_i \frac{q_i v_i^2}{\sum_i q_i v_i}$$

measured at 295 K was found to be 8.1 $nm^3$.

The ratio $v_{LA}/v_{HA} > 2$ indicates that the sintering process is fusion controlled.

## 4. Thermal Decomposition of $Fe(CO)_5$/NaY Adducts under Static Conditions

NaY zeolite saturated with $Fe(CO)_5$ shows an ivory-like colour. If the sample is heated up slowly under vacuum in the shallow bed mode (sample FeYOSB, Table I), the colour turns to dark grey. After outgassing, the generation of iron particles

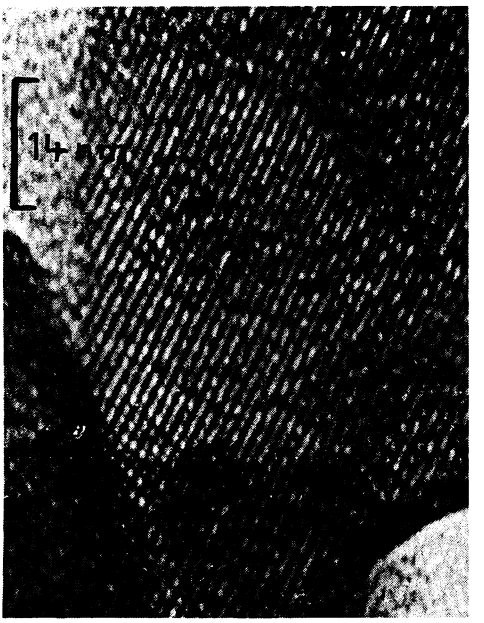

Figure 1 Electron Micrograph of NiNay: $T_R$ = 773 K. The Arrown Indicates a Lattice Defect

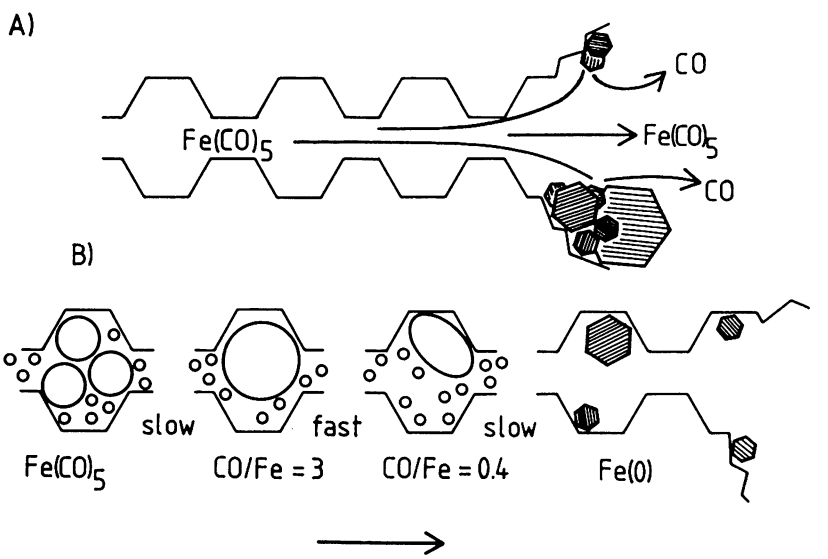


Figure 2. Model for the thermal decomposition of $Fe(CO)_5$/zeolite adducts under vacuum(A) and inert gas atmosphere(B); small circles: inert gas

with diameter greater than approximately 10 nm is found by evaluating the magnetization isotherms (10). This picture is confirmed by inspection of isolated iron zeolite crystals by TEM/EDS. The crystals show iron/silicon ratios ranging from nearly zero up to two and are covered by polycrystalline Fe (surface oxidized) particles with diameters between 20 and 50 nm, respectively.

## 5. Highly Dispersed Iron Particles by Decomposition of $Fe(CO)_5$/NaY Adducts in a Fluidized Bed

If $Fe(CO)_5$/NaY adducts are heated rapidly under fluidized bed conditions (FeY480FB, FeY17FB, FeY0FB, see Table I), at a certain temperature the ivory like colour suddenly changes to dark grey within a few seconds. The starting temperature for this fast reaction ranges from 410 K to 440 K going from the FeY0FB to the FeY480FB samples. After outgassing the iron weight content amounts to 10 wt %. Iron particle size distributions in these samples obtained from magnetization measurements are given in Table III (a).

Great differences are found for the fraction of particles exceeding 1.27 nm, which approximately is the diameter of the faujasite supercage:

- As a result of vacuum decomposition (Table III, FeY0FB), 25% of the iron phase consists of particles larger than 1.27 nm and up to 10 nm.
- A smaller amount of these large particles is formed under 17 mbar of helium (FeY17FB): only 19% of the iron phase exhibits diameters between 1.6 and 10 nm, respectively.
- A distinctly positive effect of inert gas atmosphere on the iron dispersion shows up when decomposition occurs under 480 mbar of helium (FeY480FB): the iron phase nearly completely consists of particles smaller than the size of the supercage. Only 2.7% of the iron is found to have dimensions greater than 1.6 nm.

For all samples decomposed under fluidized bed conditions, the iron fraction encaged inside the zeolite matrix shows a size distribution down to the theoretical limit of a three-dimensional cluster.

If the iron zeolites formed during fluidized bed decomposition are subjeced to prolonged heating at 550 K in the sealed ampoule, the original particle size distribution remains almost constant. After 6 hours heating at this temperature, even the highly dispersed sample proves to be stable against sintering (Table III) (b)).

## 6. A Model for the Thermal Decomposition Process of $Fe(CO_5$/NaY Adducts

The supercages of the NaY zeolite were found to be filled completely with three $Fe(CO)_5$ molecules upon saturation (11). A relatively strong complex-matrix interaction leads to increased thermal stability of the adduct compared to the free complex (12,13,14). This interaction is not sufficiently strong, however, to prevent the carbonyl from partial desorption upon heating under vacuum (12,14,15).

Two slow processes of decomposition at low and high temperatures, separated by a fast endothermic reaction, have been distinguished by thermogravimetry (14). The fast reaction starts at a CO/Fe ratio equal to $3 \pm 0.5$ and leaves relatively thermostable species with CO/Fe equal to $0.4 \pm 0.2$, which strongly interact with the matrix. From i.r. results, these two intermediate phases are assigned to species bearing bridged CO and to highly unsaturated $Fe_x(CO)_y$ clusters, respectively. The slow departure of the first CO ligands upon heating is in line with high dissociation energies determined for the first bond scission (16,17).

Table III Approximate PSD of Fe(O) in Y zeolite after decomposition of the $Fe(CO)_5$/NaY adduct in a fluidized bed under different atmospheres (a) and after sintering at 553 K for 6 hours (b)

| Particle size $v^{1/3}$ /nm | Amount of particles in each size fraction /wt % | | | | | |
|---|---|---|---|---|---|---|
| | FeYOFB[c] | | FeY17FB[c] | | FeY48OFB[c] | |
| | (a) | (b) | (a) | (b) | (a) | (b) |
| 0.33 | 45. | 34. | 26. | 26. | 57. | 55. |
| 0.56 | 6.5 | 14. | 23. | 22. | 14.6 | 16. |
| 0.91 | 19. | 21. | 32. | 29. | 2.8 | 4.0 |
| 1.0 | | | | | 20. | 20. |
| 1.27 | 4.4 | 7.8 | 0 | 4.1 | 2.8 | 3.0 |
| 1.63 | 10.1 | 6.0 | 0 | 0 | 0.5 | 0.5 |
| 2.0 | | | | | 0.3 | 0.4 |
| 2.5 | | | | | 0.9 | 1.0 |
| 3.6 | 3.6 | 3.9 | 10.3 | 8.7 | | |
| 6.0 | 9.5 | 7.6 | 8.1 | 9.2 | 1.0 | 0.1 |
| 9.4 | 2.2 | 5.8 | 0.6 | 1.6 | | |

[c] preparation conditions are given in Table I

dashed line: approximated supercage dimensions

Alternatively, an autocatalytic step may be involved in thermal decomposition of $Fe(CO)_5$ (18), since the complex was observed to decompose at iron surfaces already at 333 K (19). A model is proposed for the thermal decomposition of $Fe(CO)_5$/NaY adduct, taking into account the results discussed.

- Under vacuum (Fig. 2a), a great amount of $Fe(CO)_5$ adsorbed moves along the channels and passes lattice defects or the crystal surface upon heating. Due to the autocatalytic effect of iron, initially generated iron nuclei act as agglomeration centres for the carbonyl molecules. The formation of large iron particles as well as considerble loss of iron are the result of this effect.
- A sufficiently high inert gas pressure leads to a limited mean free path of the carbonyl molecules (Fig. 2b). Due to the restricted mobility, only a small fraction reaches places where agglomeration can occur; most molecules are thus decomposed to highly unsaturated intermediates (CO/Fe = 0.4) inside the zeolite lattice. These 'anchored' species hardly undergo further fusion until they are completely decomposed to metallic iron. The use of fast heating rates and homogeneous bed temperatures as well as fast gas exchange by application of fluidized bed conditions improve the dispersion.

These highly dispersed iron systems are surprisingly stable against sintering even at 550 K. Since much greater, graphite supported iron particles were reported to sinter already above 450 K (20), the present results clearly stress the unique stabilizing function of an intact zeolite matrix.

## CONCLUSIONS

Magnetic isotherms have been used to characterize highly dispersed Ni- and Fe-phases on zeolites in the nm range. Ni(II) exchanged NaA, NaX, NaY and NaM zeolites reduced by hydrogen between 573 and 823 K exhibit a bidisperse Ni phase. The amount and the volume of particles exceeding the cage dimensions increases in the sequence of the zeolites: M < Y < X < A. The growth of the particles is mainly controlled by the concentration of lattice defects in the matrix. Particle fusion is found to be the rate determining step. The fraction of the small particles remains nearly constant as a result of competition between further reduction and sintering.

Y zeolites saturated with iron pentacarbonyl via the gas phase proved to be suitable precursors for highly dispersed iron systems. A particular preparation method, including fast thermal decomposition of the adducts in a fluidized bed under inert atmosphere, provides the best dispersion. About 97 wt% of the iron phase is accommodated in the supercages of the zeolite. The iron systems are stable against sintering at typical CO hydrogenation reaction temperatures due to the zeolite pore structure. Work is in progress to determine the influence of different zeolite pore dimensions on particle size, stability, and catalytic behaviour of iron model catalysts.

## ACKNOWLEDGMENTS

The authors are grateful to Prof. Gunsser for his interest. T. B. is indebted to Prof. J. W. Geus for very fruitful discussions. He acknowledges a research grant from the 'Alfried Krupp von Bohlen and Halbach-Stiftung'.

P. A. J. acknowledges a research position as 'Senior Research Associate' from NFWO-FNRS (Belgium).

The help of Dr. L. Rodrique (UCL Belgium) in the microprobe analysis is appreciated. We thank cand. chem. M. Bauer for the performance of several magnetic measurements.

REFERENCES

1. H. Heinemann, Catal. Rev., Sc. & Eng., 23 (1981), 315.

2. P. A. Jacobs in "Metal Microstructures in Zeolites", Ed.: P. A. Jacobs et al. Elsevier (1982), 71.

3. F. Schmidt, W. Gunsser, J. Adolph, ACS Symposium Series, 40 (1977), 291.

4. F. Schmidt in "Metal Microstructures in Zeolites", P. A. Jacobs et al., eds, Elsevier, (1982) 191.

5. B. Pulvermacher and E. Ruckenstein, J. Catal., 35 (1974) 115.

6. B. Pulvermacher and E. Ruckenstein, J. Catal., 29 (1973) 224.

7. J. R. Anderson, "Structure of Metallic Catalysts", Academic Press, (1975) 280.

8. P. C. Flynn and S. E. Wanke, J. Catal., 34 (1974) 390, P. C. Flynn and S. E. Wanke, J. Catal., 34 (1974) 400.

9. E. Garbowski, C. Mirodatos and M. Primet, in "Metal Microstructures in Zeolites", P. A. Jacobs et al., eds., Elsevier, (1982) 235.

10. F. Schmidt, W. Gunsser and A. Knappwost, Z. Nat. forsch., 30a (1975) 1627.

11. Th. Bein, P. A. Jacobs and F. Schmidt, in "Metal Microstructures in Zeolites", P. A. Jacobs et al., eds. Elsevier, (1982) 111.

12. J. B. Nagy, M. Van Eenoo, E. G. Derouane, J. Catal., 58 (1979), 230.

13. Th. Bein and P. A. Jacobs, J. Chem. Soc., Faraday Trans., 1, (1983), in press.

14. Th. Bein and P. A. Jacobs, submitted to J. Chem. Soc., Faraday Trans., 1.

15. D. Ballivet-Tkatchenko and G. Coudurier, Inorg. Chem., 18 (1979) 558.

16. G. P. Smith and R. M. Laine, J. Phys. Chem., 85 (1981) 1620.

17. P. C. Engelking and W. C. Lineberger, J. Am. Chem. Soc., 101 (19) (1979) 5570.

18. A. Brenner and D. A. Hucul, Inorg. Chem., 18 (10) (1979) 2836.

19. A. Mittasch, Z. ang. Ch., 41 (1928) 831.

20. J. Phillips, B. Clausen, J. A. Dumesic, J. Phys. Chem., 84 (1980), 1814.